Charge Transport in Arrays of Semiconductor Gamma-Ray Detectors

H. H. Barrett, J. D. Eskin, and H. B. Barber
Department of Radiology and Optical Sciences Center, University of Arizona, Tucson, Arizona 85724
(Received 27 December 1994)

We analyze the effects of electrode size on performance of arrays of semiconductor gamma-ray detectors, especially when there is significant charge trapping. With large electrodes, motions of holes and electrons are of equal importance, but when the positive electrode is segmented into an array of small elements the contributions of holes to the output, and hence the effects of hole trapping, are much less significant. The implications of this analysis for the design of practical detector arrays are discussed, and some preliminary experimental verification of the theory is presented.

PACS numbers: 07.85.Fv, 29.40.Wk, 72.20.Jv, 87.62.+n

Gamma-ray detector arrays are important tools in high-energy physics, nuclear spectroscopy, nondestructive testing, gamma-ray astronomy, and medical imaging. Semiconductor detectors are advantageous for these applications because of their good energy resolution and the ability to fabricate compact arrays with very small elements. In imaging applications, the detector elements are referred to as picture elements or *pixels*. One important gamma-ray imaging application for which semiconductor arrays are currently receiving considerable attention is single-photon emission computed tomography (SPECT), a nuclear-medicine technique where a three-dimensional map of the concentration of a radiotracer is formed. It has recently been demonstrated that reduction in pixel size allows important improvements in sensitivity and spatial resolution of the final image in this application [1].

Various semiconductor materials have been used in gamma-ray detector arrays. Silicon and germanium have excellent energy resolution and charge-transport properties, but low atomic number, so they do not effectively absorb high-energy gamma rays. Because of its small band gap, germanium must be operated at cryogenic temperature. Recent research has concentrated on materials with high atomic number and large band gaps; examples include mercuric iodide (HgI_2) [2], cadmium telluride (CdTe) [3], and cadmium-zinc telluride ($Cd_{1-x}Zn_xTe$, $x \simeq 0.04$–0.2) [4]. Though these materials operate at room temperature and are usable for gamma-ray energies up to several hundred keV, they do not have the desirable charge-transport characteristics of Si or Ge. The carrier mobilities are lower, and the carriers are trapped at impurities or defects. Both of these effects are usually more serious for holes than for electrons. Because of the trapping, the total charge induced in an integrating readout circuit depends on the depth at which the gamma ray is absorbed. As a result, the pulse-height spectra of these materials typically show a tail or plateau, with a large fraction of the events occurring in this tail instead of in the desired photopeak [5,6]. Since events in the tail convey little useful energy information, some of the advantages of semiconductor detectors are negated by hole trapping.

The induced currents due to charge motion in vacuum were analyzed in classic papers by Shockley [7] and Ramo [8]. Ramo introduced the concept of a "weighting potential," applied by later authors to gas and solid-state radiation detectors [9–13]. An important line of investigation [14] attempts to devise detector geometries in which the detected signal results primarily from electron transport. A practical demonstration of this possibility was the recent paper by Luke [15] on a solid-state counterpart of Frisch grids [16], developed originally for gas detectors.

The purpose of this Letter is to demonstrate theoretically and experimentally that semiconductor detector arrays can be made relatively insensitive to hole trapping by the simple expedient of properly choosing the pixel size. The method of calculation is the classic electrostatic Green's function, but it is easy to show that the results are equivalent to what would be obtained by use of the Ramo-Shockley theorem and weighting potentials [17].

We consider a homogeneous slab of high-resistivity semiconductor of thickness L. The lateral dimensions of the slab are much larger than L and assumed to be infinite. On one side of the slab is a continuous metal electrode covering the entire area and maintained at potential V_0; on the other side is a metal electrode segmented into an array of individual square pixels of size $\epsilon \times \epsilon$. There is a gap of negligible dimension between the pixel electrodes, but no other mechanical or electrical separation of the pixels is employed. Each pixel is connected to a separate amplifier of very low input impedance which maintains the electrode at zero potential. The basic electrostatic model is thus nothing more than a parallel-plate capacitor, except that current through individual pixels can be measured separately. A practical device that closely matches this model is under investigation in our laboratory [18].

Using this model, we now calculate the current that flows in each pixel after absorption of a gamma ray. We assume the gamma ray is absorbed at time $t = 0$ and at point (x_i, y_i, z_i), where x_i and y_i are in the plane of the slab and z_i is measured from the segmented electrode. The gamma ray is assumed to interact with the semiconductor by a photoelectric process, with the

 0031-9007/95/75(1)/156(4)$06.00

photoelectron producing N_0 hole-electron pairs within a short distance of the initial interaction point. Both the finite range of the photoelectron and the small statistical fluctuations in N_0 are neglected here but will be considered in a later publication.

The electrons drift towards the positive electrode at speed $v_e = \mu_e E$ while the holes drift towards the negative electrode at speed $v_h = \mu_h E$, where μ_e and μ_h are the electron and hole mobilities, respectively, and $E = V_0/L$ is the applied electric field. For reasons that will become apparent shortly, we assume that the segmented electrode is the positive one, but the analysis is easily modified for the opposite case. As the carriers drift, some of them are trapped, and the total volume charge density must include the immobile trapped component as well as the drifting carriers. We neglect diffusion of the carriers since we can show that the diffusion length is negligible compared to typical pixel dimensions over the drift time [19], and we neglect detrapping of the charge carriers. With these assumptions, the total time-dependent charge density for electrons (both trapped and free) is given by

$$\rho_e(x,y,z,t) = -eN_0\delta(x-x_i)\delta(y-y_i)\{\exp(-t/\tau_e)\delta[z-(z_i-v_e t)] + (1/v_e\tau_e)\exp[(z-z_i)/v_e\tau_e]\,\mathrm{rect}[(z-(z_i-\tfrac{1}{2}v_e t))/v_e t]\}, \quad (1)$$

where τ_e is the trapping-limited electron lifetime $\mathrm{rect}(u) = 1$ if $|u| \le \frac{1}{2}$, 0 if $|u| > \frac{1}{2}$, and $\delta(\cdot)$ is the Dirac delta function. A similar expression gives the charge density for holes.

The next task is to compute the current in the external circuit as a result of the carrier motion. This is very easy to do for large electrodes; a simple conservation-of-energy argument [20] shows that a single carrier moving a distance Δx in time Δt induces (on average) a current $I(t) = e\,\Delta x/L\,\Delta t$ in the electrode during this time. The total induced charge, which is the quantity of interest if an integrating or charge-sensitive amplifier is used, is $e\,\Delta x/L$. If an electron-hole pair is created at depth z_i and there is no trapping, the hole moves a distance $L - z_i$ and contributes $e(L - z_i)/L$ to the charge, while the electron moves a distance z_i and contributes ez_i/L, so the total charge is e per electron-hole pair. On the other hand, if the hole is immediately trapped ($v_h\tau_h \ll L$), then there is essentially no hole contribution, and the total induced charge can vary from 0 to e depending on the random depth of interaction. This is the origin of the tail mentioned in the introduction.

The conservation-of-energy argument is not applicable with segmented electrodes since it gives only the total current that flows in the external circuit, not the fraction that flows through a single pixel. To study the output from an individual pixel, we solve Poisson's equation $\nabla^2\phi = -\rho/\epsilon$ and use the solution to determine the normal derivative of the time-varying potential at all points on the surface of a single pixel electrode. By Gauss's law, this normal derivative implies a time-varying surface charge density on the pixel, and an integral over the area of the pixel gives the total induced charge on the pixel as function of time. From this expression current-vs-time wave forms or total collected charge on the pixel can be computed.

The Green's function for this problem can be computed as an infinite series of pairs of image charges, with the result [21]

$$G(x,y,z;x_0,y_0,z_0) = \sum_{k=-\infty}^{\infty}\left[\frac{1}{\sqrt{(z-2kL-z_0)^2+r^2}} - \frac{1}{\sqrt{(z-2kL+z_0)^2+r^2}}\right], \quad (2)$$

where $r^2 = (x-x_0)^2 + (y-y_0)^2$. The sum in Eq. (2) converges rapidly and satisfies Dirichlet boundary conditions. As a check, we have verified that this Green's function leads to the expected linear variation of potential with z in the absence of volume charge.

The remainder of the calculation is a standard exercise in electrostatics [22]. The results include current wave forms and total induced charge as a function of electron and hole mobilities and trapping lifetimes, depth of interaction of the gamma ray, and size of the pixel. From these results, expected pulse-height spectra can be computed.

Figure 1 shows calculated integrated-current wave forms for two different pixel sizes and three depths of interaction. With large pixels and no trapping, the currents are constant until the carriers have drifted completely across the slab. This numerical result, which is in complete accord with the standard conservation-of-energy argument, provides another cross-check on the Green's function method. For small electrodes, the standard method does not work, and our approach gives new results. If the pixel size is $\epsilon \times \epsilon$, a drifting electron does not make much contribution to the current through a particular pixel until it comes within a distance $z \simeq \epsilon$ of that pixel. As a result, the current wave form shows a sharp peak near the end of the drift. If there is no trapping, the total induced charge Q_{tot} (the integral under the current wave form) is just e per electron-hole pair as expected, providing yet another check on the theory.

If there is trapping, striking differences between large and small pixels emerge. Figure 2 shows the relative fraction of Q_{tot} contributed by electrons and holes for

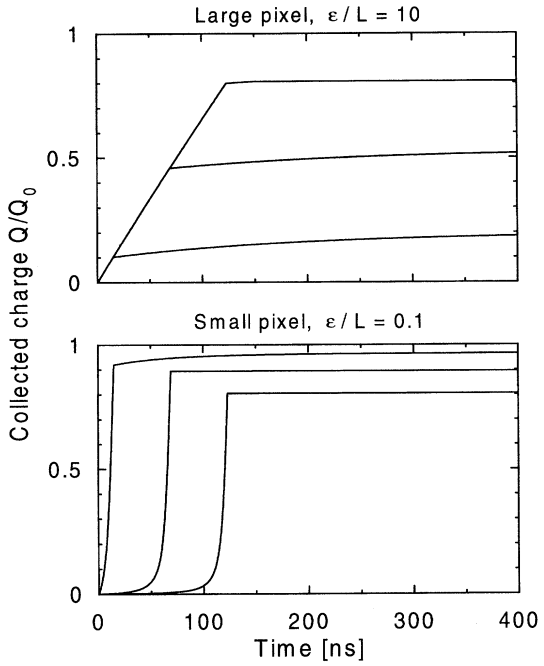

FIG. 1. Collected charge vs time for different pixel sizes. These wave forms are calculated for interaction points directly over the center of the pixel and for positive bias on the pixel electrode. Therefore, in the absence of trapping, the electron will strike the center of the pixel. The interaction depths are at $z_i = 0.2L$, $0.5L$, and $0.8L$.

different pixel sizes and interaction depths. It is seen that holes are quite unimportant if the signal is sensed on a small positive electrode. Therefore, if holes are trapped more strongly than electrons, the total signal is far less dependent on depth of interaction with small pixels than with large ones.

These predictions were tested experimentally with a 1.5 mm thick slab of $Cd_{0.8}Zn_{0.2}Te$. In this material the electron drift length ($\mu_e\tau_e E$) is typically about 2 orders of magnitude larger than the hole drift length. For the specific material used in the experiments reported here, $\mu_e\tau_e E$ is about $20L$ while $\mu_h\tau_h E$ is only about $0.16L$ for $V_0 = 200$ V and $L = 1.5$ mm. Thus most of the electrons will drift all the way across the crystal and contribute fully to the output, but holes are strongly trapped. One side of the slab is covered with a continuous metal film, used as the negative electrode. The other side has a 48×48 array of small pixels, each 0.125×0.125 mm. Each electrode is connected via indium-bump bonding to a matching pad on an interconnection device called a fanout. The fanout allows various contiguous subsets of the pixels to be connected together electrically, forming larger composite pixels ranging in size from 0.25 mm to 2.5 mm. We thus have available on a single slab pixels much smaller than the slab thickness and ones almost twice as large as the thickness.

Extensive measurements on this device have been made. Current wave forms have been observed with both gamma-

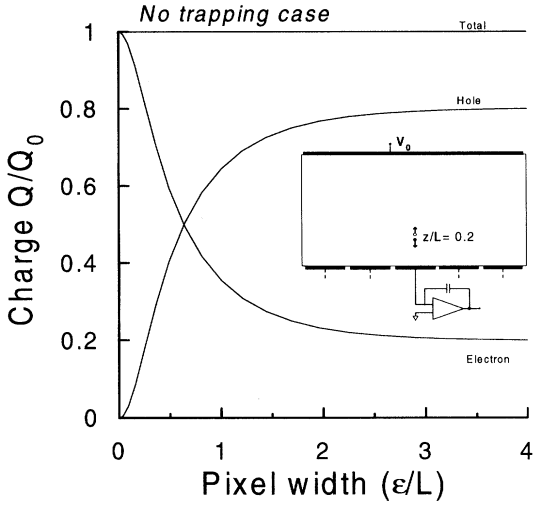

FIG. 2. Total collected charge for holes and electrons absorbed at depth $z_i = 0.2L$ as a function of pixel size.

ray and alpha-particle excitation, and pulse-height spectra have been recorded under a variety of conditions. A full report on these studies will be published separately, but Fig. 3 illustrates one of the most important results. To obtain the experimental spectra shown there, the crystal was irradiated with uncollimated 140 keV photons from ^{99m}Tc. Each composite pixel was connected to standard pulse electronics, and the spectrum was recorded on a multichannel analyzer. The simulated spectra were calculated by use of the Green's function model described in the text, with gamma-ray interactions randomly distributed within the volume of the crystal according to an exponential law, with the attenuation coefficient appropri-

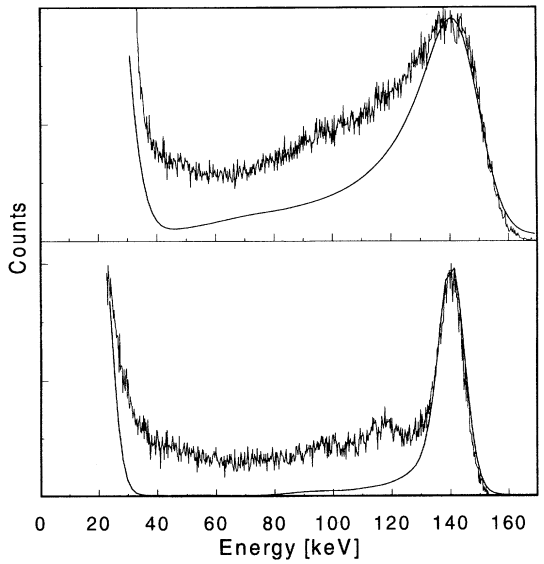

FIG. 3. Theoretical and experimental pulse-height spectra for two different pixel sizes, $\epsilon = 1.25$ mm (top) and 0.375 mm (bottom). A weak K-escape peak seen in the experimental spectra is not accounted for in the theory.

ate to 140 keV. Measured $\mu\tau$ values were used. A constant electronic noise was assumed, with the standard deviation adjusted to approximately match the measured spectra. There were no other adjustable parameters in the calculation.

It is evident from Fig. 3 that the tail effect is very severe with a large pixel but greatly reduced with a smaller one. Though not shown here, experiments with still smaller pixels showed a larger tail. The 0.375 mm pixel shown in Fig. 3 gave the best measured spectrum. The theory qualitatively predicts the experimental spectra but underestimates the tail somewhat. The discrepancy between theory and experiment is probably because the theory takes no account of charge diffusion and the finite volume over which the initial charge is created, effects that become more pronounced for small pixels. Further investigations will refine the theory by accounting for these effects.

In conclusion, we have shown that the deleterious effects of hole trapping are greatly reduced if the positive electrode is divided into an array of small pixels. Then hole transport contributes relatively little to the measured signals and the tail in the pulse-height spectrum is reduced significantly. This result is important in terms of both efficiency and energy resolution of the detectors. In the past, detectors made of materials such as CdTe and CdZnTe had to be thin in order to get good hole collection, or else the user had to accept a poor spectrum with few events under the photopeak. In either case, the photopeak efficiency of the detector was poor except for gamma rays of very low energy. The theory presented here shows that thick detectors can be used with small pixels without sacrificing photopeak efficiency.

Several practical design rules for array detectors follow from the analysis given here. One is that the segemented electrode should always be the positive one if hole trapping is stronger then electron trapping, as it usually is. Another is that the detector thickness should be several times larger than the pixel size, allowing the detector to have good stopping power. The analysis also suggests that row-by-column readout is likely to encounter difficulties with materials such as CdZnTe. The negative electrodes will give poor spectra because of the hole trapping, and the signals may be too weak even for determination of position. A pixel-based readout scheme is much more attactive in these materials. Finally, designers of pulse electronics for array detectors should be aware of the faster rise time and reduced dependence on depth of interaction when small pixels are used.

We wish to thank Hughes Aircraft Company, and, especially, John Venzon and William Hamilton for loaning us the fanout device. We also thank Digirad Inc. and Patrick Doty for supplying the CdZnTe material and assistance in its optimal use. At the University of Arizona, Erick Young provided invaluable technical assistance, and James Woolfenden provided the overall leadership that made this work possible. Conversations with S. Augustine and L-A. Hamel also provided considerable insight. This work was supported by NIH Grant No. CA23417.

[1] M. M. Rogulski, H. B. Barber, H. H. Barrett, R. L. Shoemaker, and J. M. Woolfenden, IEEE Trans. Nucl. Sci. **40**, 1123 (1993).
[2] B. E. Patt, A. Del Duca, R. Dolin, and C. Ortale, IEEE. Trans. Nucl. Sci. **33**, 523 (1986).
[3] E. Raiskin and J. F. Butler, IEEE Trans. Nucl. Sci. **NS-35**, 82 (1988).
[4] J. F. Butler, C. L. Lingren, and F. P. Doty, IEEE Trans. Nucl. Sci. **NS-37**, 605 (1992).
[5] H. B. Barber, H. H. Barrett, G. Entine, T. S. Hickernell, D. P. Kwo, C. Ortale, and J. M. Woolfenden, Med. Phys. **18**, 373 (1991).
[6] W. Akutagawa and K. Zanio, J. Appl. Phys. **40**, 3838 (1969).
[7] W. Shockley, J. Appl. Phys. **9**, 635 (1938).
[8] S. Ramo, Proc. IRE **27**, 584 (1939).
[9] C. K. Jen, Proc. IRE **29**, 345 (1941).
[10] G. Cavalleri, G. Fabri, E. Gatti, and V. Svelto, Nucl. Instrum. Methods **21**, 177 (1963).
[11] F. S. Goulding, Nucl. Instrum. Methods **43**, 46 (1966).
[12] M. Martin and G. Ottaviani, Nucl. Instrum. Methods **67**, 177 (1969).
[13] W. C. Sailor, H.-J. Ziock, W. W. Kinnison, and K. Holzscheiter, Nucl. Instrum. Methods Phys. Res. Sect. A **303**, 285 (1991).
[14] H. L. Malm, C. Canalli, J. W. Mayer, M-A. Nicolet, K. R. Zanio, and W. Akutagawa, Appl. Phys. Lett. **26**, 344 (1975).
[15] P. N. Luke, Appl. Phys. Lett. **65**, 2884 (1994).
[16] O. Frisch, British Atomic Energy Report No. BR-49, 1944 (unpublished).
[17] The weighting potential, commonly used in this literature, is $1/4\pi$ times the integral over the electrode of the normal derivative of the Green's function.
[18] H. B. Barber, H. H. Barrett, E. L. Dereniak, N. E. Hartsough, D. L. Perry, P. C. T. Roberts, M. M. Rogulski, J. M. Woolfenden, and E. T. Young, IEEE Trans. Med. Imaging **40**, 1140 (1993).
[19] Carrier diffusion is insensitive to the properties of the specific semiconductor material. The diffusion constant is linearly related to the mobility by the Einstein relation [see, for example, N. W. Ashcroft and N. D. Mermin, *Solid State Physics* (Sanders, Philadelphia, 1976)], so materials in which carriers diffuse rapidly also have large drift velocities, and hence less time to diffuse. Total spread depends on thickness and bias voltage but not on mobility. For example, rms spreading in a 1 mm thick detector (of any material) at 100 V bias is about 23 μm. See H. G. Spieler and E. E. Haller, IEEE Trans. Nucl. Sci. **NS-22**, 419 (1985).
[20] G. F. Knoll, *Radiation Detection and Measurement* (Wiley, New York, 1989), 2nd ed., pp. 403–405.
[21] O. D. Kellogg, *Foundations of Potential Theory* (Ungar, New York, 1929), p. 230.
[22] The time-dependent terms in Maxwell's equations are negligible if the carrier velocities are much less than c, a condition that is easily satisfied in practice.